Reynolds number effects in a turbulent pipe flow for low to moderate Re

Reynolds number effects in a turbulent pipe flow for low to moderate Re

J. M. J. den Toonder[a] and F. T. M. Nieuwstadt
Laboratory for Aero- and Hydrodynamics, Delft University of Technology, Rotterdamseweg 145, 2628 AL Delft, The Netherlands

(Received 31 July 1995; accepted 19 June 1997)

We present in this paper high resolution, two-dimensional LDV measurements in a turbulent pipe flow of water over the Reynolds number range 5000–25000. Results for the turbulence statistics up to the fourth moment are presented, as well as power spectra in the near-wall region. These results clearly show that the turbulence statistics scaled on inner variables are Reynolds-number dependent in the aforementioned range of Reynolds numbers. For example, the constants in the dimensionless logarithmic mean-velocity profile are shown to vary with Reynolds number. Our conclusion that turbulence statistics depend on the Reynolds number is consistent with results found in other flow configurations, e.g., a channel flow. Our results for the pipe flow, however, lead nevertheless to quite different tendencies. © *1997 American Institute of Physics.* [S1070-6631(97)03711-2]

I. INTRODUCTION

Wall-bounded turbulent flows, such as pipe flows, channel flows and boundary layers, are generally believed to consist of several regimes, each having their own flow characteristics and scaling parameters. In the conventional picture a distinction is made between a so-called inner and an outer layer. The inner layer consists of the near-wall region, in which the flow is assumed to be independent of the large-scale geometry. In other words, the flow quantities in the inner layer are similar regardless of the type of flow geometry, whether this is a pipe, a channel or a flat plate. The outer layer on the other hand depends on the geometry of the flow. Of course, a region of overlap between both layers exists in which a gradual transition from one layer into the other should occur.

The classic idea behind the scaling is that turbulence quantities (e.g. mean velocity, rms-velocity fluctuations, power spectra), if properly scaled, should collapse onto a single curve independent of the Reynolds number. For the inner layer it then also follows that this similarity curve should be independent of the flow geometry.

The appropriate scaling parameters for the inner region for the case of a smooth wall, are called the ''inner variables.'' They are the viscosity, ν and the friction velocity u_τ, which is defined as $u_\tau=(\tau_w/\rho)^{1/2}$, where ρ is the density of the fluid and τ_w is the mean shear stress at the wall. For example, inner scaling demands that the mean-velocity profile should obey the unique relationship

$$U^+=f(y^+), \tag{1}$$

where $U^+=U/u_\tau$ is the scaled mean velocity and $y^+=yu_\tau/\nu$ is the dimensionless distance to the wall. The f is a universal function presumably independent of Reynolds number and generally known as ''the law of the wall.'' We will come back to this relationship in Sec. III A.

This classic notion of inner scaling has been questioned in the past, and in particular the influence of the Reynolds number on the statistical turbulence quantities has been examined for channels and boundary layers especially at low Reynolds numbers. An extensive review is given in Gad-el-Hak and Bandyopadhyay.[1] The main conclusions of that review are the mean velocity seems indeed to scale on inner variables, i.e., there appears to exist a universal mean-velocity profile in the inner layer (Bradshaw and Huang,[2] however, again question the inner-layer scaling of the mean profile); however unlike the mean flow, the turbulence statistics do not seem to scale accurately with the inner variables over the entire inner layer, but only in a very small portion adjacent to the wall. In most experiments considered by Gad-el-Hak and Bandyopadhyay,[1] the peak of the scaled stream-wise turbulence intensity increases slightly with Reynolds number, while the position of the peak remains unaffected. A recent review of experimental data by Mochizuki and Nieuwstadt,[3] on the other hand, indicates that the peak of the stream-wise velocity fluctuations stays constant for an extensive range of Reynolds numbers in both external and internal flows. In contrast to their findings on the stream-wise turbulence intensity, Gad-el-Hak and Bandyopadhyay[1] notice that the peaks of the turbulence intensity of the velocity normal to the wall, and of the Reynolds stress move away from the wall with increasing Reynolds number, and that the magnitude of the peaks increases.

It should be noted here, that many experiments in the past have a priori assumed inner scaling for the mean flow to be valid and have used the velocity data to compute u_τ. This might lead to systematic errors in the turbulence statistics plotted in wall variables and such procedure should be avoided, whenever possible, certainly in a study on Reynolds number dependence of inner scaling. However, in channel flows and boundary layers it is difficult to obtain a sufficiently accurate estimate of u_τ by measuring the pressure drop. On the other hand pipe flows have the advantage that it is much easier to measure the pressure drop and from this obtain u_τ with confidence. Furthermore, as explained in Gad-el-Hak and Bandyopadhyay,[1] many of the alleged Reynolds number effects may be attributed to the strong increase of the non-dimensional length of measurement probes as the Reynolds number increases, making the measurements at high

[a]Present address: Philips Research, Prof. Holstlaan 4, 5656 AA Eindhoven, The Netherlands; Electronic mail: toonder@natlab.research.philips.com

 1070-6631/97/9(11)/3398/12/$10.00

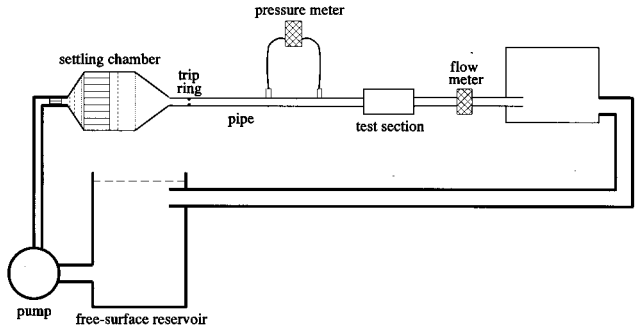

FIG. 1. The pipe flow facility. The main part is a cylindrical perspex pipe with length 34 m and inner diameter 40 mm. It contains a test section for the LDV measurements.

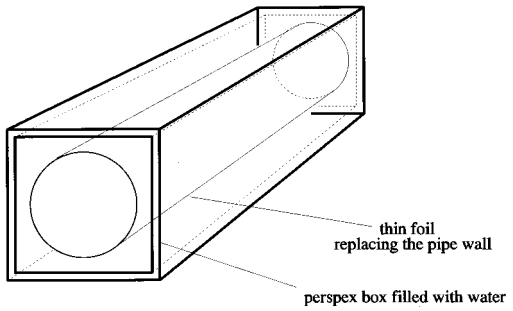

FIG. 2. The test section.

Reynolds numbers unreliable because of the loss of resolution.

The objective of the present paper is to investigate the influence of the Reynolds number on inner scaling in turbulent pipe flow for low to moderate Reynolds numbers. A systematic study of this effect is still lacking for pipe flow, contrary to channel flow (e.g., Wei and Willmarth[4]). Although Perry and Abell[5] address the issue of scaling laws for pipe-flow turbulence, they do not measure close enough to the wall, and have insufficient probe resolution to be able to prove or refute the existence of similarity in terms of inner variables. In our study we use two-component Laser Doppler Velocimetry (LDV) to measure turbulence statistics and power spectra in a turbulent pipe flow with the Reynolds number, based on bulk mean velocity and diameter (i.e., $\mathrm{Re}=U_bD/\nu$), ranging from 4900 to 25300.

The plan of the present paper is at follows. In Sec. II a description of the experiment is given, including the flow facility, the LDV setup, the experimental conditions and the data processing. We present in Sec. III the results of the measurements, which are subdivided into ''turbulence statistics'' and ''power spectra.'' Finally, Sec. IV contains the conclusions and a discussion.

II. DESCRIPTION OF THE EXPERIMENTAL SETUP

A. The pipe flow loop

The experiments were performed in the re-circulatory pipe flow facility of the Laboratory for Aero- and Hydrodynamics, a schematic diagram of which is shown in Fig. 1. An extensive description of this setup can be found in Draad.[6] The main part of the facility consists of a cylindrical perspex pipe with a length of 34 m and an inner diameter of 40 mm. After the pump and before entering the pipe, the fluid passes first through a flow straightening device and then through the settling chamber. The settling chamber contains another flow straightening device as well as several screens, and it is connected to the pipe by a smooth contraction. At a distance of 1 m behind the pipe entrance a so-called ''trip ring'' is inserted in the pipe to force transition to turbulence. This trip ring causes a sudden narrowing of the pipe diameter with a step of 6 mm, extending 5 mm in the stream-wise direction. To avoid secondary circulations due to free convection the entire pipe is insulated with 3 cm Climaflex pipe insulation.

The pressure gradient along the pipe is measured with two membrane differential-pressure transducers (Validyne Engineering Corp., type DP15–20), which are identical except for having different ranges (only one of these is sketched in Fig. 1). One transducer with a range of 88 $\mathrm{mmH_2O}$ measures the pressure difference between the positions 20 m and 31.5 m downstream of the settling chamber. The second transducer has a range of 255 $\mathrm{mmH_2O}$ and measures the pressure difference between 18 m and 28 m behind the settling chamber. The pressure taps have a diameter of 1 mm. The flow rate is measured with a magnetic inductive flow meter (Krohne Altometer, type SC 100 AS). The temperature of the fluid is measured with a thermocouple in the free-surface reservoir. This temperature is used to calculate the viscosity of water during the experiments. The measured pressure gradient, flow rate and temperature are acquired automatically with a personal computer. The pump in the system is a so-called disk pump, manufactured by Begemann.

The curvature of the pipe wall leads to the difficulty to measure very close to the wall with LDV, because of refraction of the laser beams by the pipe wall. This difficulty arises because of the differences in refractive index of the test fluid (i.e., water with $n=1.33$), the material of the pipe (i.e., perspex with $n=1.49$), and air ($n=1.0$). To minimize this problem, we have constructed a special test section, illustrated in Fig. 2. In the test section, located 30 m downstream of the inlet of the pipe, the pipe wall is partly replaced by a thin foil made of Teflon FEP (fluorised ethylene propylene) with a thickness of 190 μm, kindly provided by Du Pont de Nemours. This material has a refractive index of $n=1.344 \pm 0.003$, which is quite close to that of our test fluid, so that effects of refraction are quite small. The use of this foil in combination with the square perspex box filled with water around the cylindrical foil minimises the refraction of the laser beams. As a result we can perform measurements down to a distance of 0.2 mm from the wall, which varies for our measurements between 1.7 and 6.8 viscous wall units. The inner diameter of the pipe segment formed by the foil is 40.37 mm. The walls of the perspex box have a thickness of 6 mm while the distance of these walls to the pipe centre is 60 mm.

Despite this care taken in constructing the test section, it turned out that very close to the wall sources of measurement

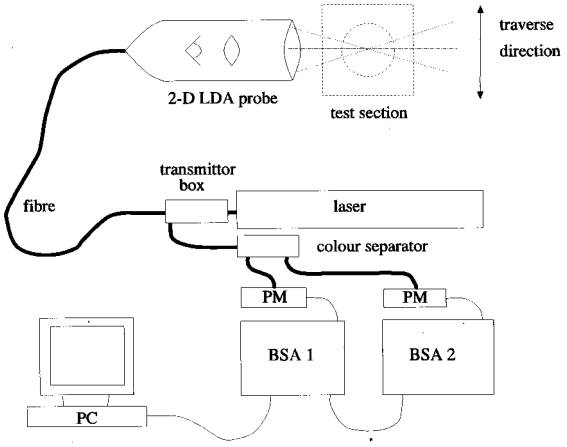

FIG. 3. The LDV setup used is a two-colour backscatter system supplied by Dantec. The received signal is processed by two Burst Spectrum Analyzers.

error were present. These sources showed up as scatter in the second and higher statistical moments, in particular for the radial velocity component, at measurement positions smaller than $y^+=5$. The scatter could not be explained by a lack of sufficiently many independent samples to compute the moments; in other words statistical inaccuracies were not the cause of the scatter. It is most probable that reflections of the laser light from the pipe wall that were picked up by the receiving optics have been the cause of the inaccuracies in the second and higher moments in the region $y^+<5$. The vertical laser beam pair (see the next section), measuring the radial velocity component, is most sensitive to such disturbances. Because of this scatter, we decided to leave the data measured at positions further from the wall than $y^+=5$ out of the results to be presented in Sec. III. It will be clear from the results in Sec. III that the data outside the layer $y^+<5$ do not suffer from large error sources, and have actually quite good accuracy.

B. The LDV setup

Laser Doppler Velocimetry (LDV) is a well-established technique for measuring turbulent flows. An exposition of the general principles can for instance be found in Durst *et al.*[7] or Ruck.[8]

The LDV setup used in our experiments is sketched in Fig. 3. The measurements were performed with a 2-component LDV system manufactured by Dantec. This system uses two orthogonal pairs of laser beams with pairwise light of a different wavelength to measure the fluid-velocity in two directions. Each of the pairs forms a so-called ''measurement volume'' at the position where the two beams intersect. The light that is scattered by a particle travelling through the measurement volume is gathered in the backscattered direction. The optics to focus the laser beams into the pipe and also to receive the scattered light are built in one measuring probe (Dantec), having a focusing front lens with focal length 80 mm. This probe is attached to a three-dimensional (3-D) traversing system also supplied by Dantec. The probe is connected to an argon–ion laser of Spectra Physics (model 2020) via a fiber and a transmittor box. The transmittor box splits up the light that is produced by the laser into two wavelengths, namely 514.5 nm and 488 nm (one for each laser beam pair), and feeds it into the fiber through which the light travels to the measuring probe. At the same time, the fibre carries the backscattered laser light from the probe back to two photo-multiplier (PM) tubes, via the transmittor box and a colour separator that separates the two colours. The output from the PM tubes goes to two ''Burst Spectrum Analyzers'' (Dantec, type Enhanced 57N20 and Enhanced slave 57N35), one for each laser beam pair, or velocity component. By means of a spectral analysis of the signal, each BSA computes the Doppler shift between the transmitted and the scattered light, and this shift is proportional to the velocity component of the particle perpendicular to both beams.

The stream-wise (or axial) velocity component was measured using the 488 nm laser beam pair, and the normal (or radial) component with the 514.5 nm pair. That means that the 514.5 nm pair lay in the plane perpendicular to the stream-wise direction (i.e., the ''vertical pair''), and the 488 nm pair lay in the plane parallel to both the stream-wise direction and the optical axis of the probe (i.e., the ''horizontal pair''). Prior to the actual measurements the measurement volumes for both components were made to coincide at the same position by using a pinhole with diameter 20 μm. The paths of all four laser beams within the probe were adjusted so that they all were focused on the pinhole if this was placed in the focal point of the probe front lens in air. The dimensions of the measurement volumes are estimated to be 20, 20 and 100 μm in the stream-wise, normal and span-wise directions, respectively. That means that the width of the measurement volumes, i.e., the size perpendicular to the mean flow, varied from 0.2 to 0.6 viscous lengths in our pipe flow measurements.

In all measurements to be presented later in this paper, the probe was traversed in the vertical direction, causing the measurement volumes to travel along the vertical central axis of the pipe, as indicated in Fig. 3.

We aligned the probe in the horizontal and vertical planes with respect to the pipe by observing the reflections of the laser-beams coming from the test section. The probe was adjusted so that these reflections travelled along symmetric paths with respect to the incoming beams. Furthermore, the probe was rotated about its optical axis and fixed in the position in which the mean velocity measured with the vertical laser beam pair in the centre of the pipe was identically zero.

The actual location of the measurement volumes was determined by examining instantaneously the output of the BSA's, i.e., the Doppler signal, with a digital scope while traversing the probe. When the measurement volumes hit the foil, this shows up as a sudden increase in the noise level of the observed signal. In this way, the location of the wall was determined at four positions from which the zero position of the probe was determined.

In all experiments the fluid was seeded with pigment on TiO_2-basis to get sufficiently high data rates (see Sec. II C). The power supplied by the laser was always 2.5 W, corresponding to a power of approximately 150 mW in each laser beam.

TABLE I. Experimental conditions of the measurements. Each symbol (first column) corresponds to one full profile or spectrum measurement, and will also be used in the figures in this paper to denote the corresponding measurement.

Experimental conditions of the profile measurements				
Symbol	u_τ (mm/s)	ν/u_τ (mm)	Re	Re_τ
○	9.2	0.120	4900	338
▲	16.9	0.064	10000	629
■	27.8	0.039	17800	1040
+	37.3	0.029	24600	1380

Experimental conditions of the spectrum measurements						
Symbol	u_τ (mm/s)	ν/u_τ (mm)	Re	Re_τ	y^+	
○	8.8	0.116	5100	348	12.1	30.2
▲	15.6	0.064	10000	630	12.0	30.0
+	35.0	0.029	25300	1413	11.9	30.1

The BSA's and the traversing system are controlled by a PC, making fully automatic measurements possible.

C. The experimental conditions and data processing

We performed two types of measurements: ''profile measurements,'' from which turbulence statistics as a function of wall distance were determined, and ''spectrum measurements'' for the computation of power spectra. This section contains a description of the experimental conditions. All the measurements were carried out with ''Delft'' tap water. Table I lists the experimental conditions of the measurements. In the first column the symbols are shown which we will use in the figures in the remainder of this paper for the corresponding measurements.

The friction velocity was determined from the pressure measurements according to

$$u_\tau = \sqrt{\frac{D}{4\rho}\left|\frac{\Delta P}{\Delta z}\right|}, \tag{2}$$

where D is the diameter of the pipe, ΔP is the measured pressure difference and Δz is the distance over which ΔP is measured. For the first two profile measurements (i.e., the two lowest Re) in Table I the 88 $\mathrm{mmH_2O}$ pressure transducer was used, in the other cases the 255 $\mathrm{mmH_2O}$ transducer. The relative measurement error in u was 0.3%, as estimated from Eq. (2) and uncertainties in the quantities D, ρ, ΔP and Δz.[9]

The viscous length scale ν/u_τ is composed of the kinematic viscosity of the fluid, ν, determined at the observed temperature, and the friction velocity. The variation of the temperature of the fluid during each profile measurement was less than 0.1 °C, with a mean value between 16.3 °C and 17.0 °C.

The Reynolds number Re is defined with the bulk velocity in the pipe, i.e. $\mathrm{Re}=U_b\,D/\nu$, where U_b is determined from the measured flow rate Q. The Reynolds number Re_τ is defined with the friction velocity: $\mathrm{Re}_\tau=u_\tau\,D/\nu$.

Profile measurements were conducted at four different Reynolds numbers. One profile measurement consisted of a traverse through the pipe, measuring the velocity at a large number of positions (i.e., 35 for the lowest Reynolds number, and 70 for the highest Reynolds number) starting from the wall and moving toward the centre of the pipe. At each position samples were gathered at a certain mean data rate (f_{dr}), by operating the BSA's in the so-called dead-time mode, and during a given measuring time T. In the dead-time mode, the time separation between the samples can be fixed to a certain value (however only approximately, due to the stochastic nature of the sampling process); in this way, the mean data rate can be influenced, provided there are enough samples in the first place. For the two lowest Reynolds numbers, f_{dr} was around 30 Hz, while $T=600$ s. In the other cases $f_{dr}\approx 60$ Hz and $T=300$ s. That means that typically 18000 samples were obtained per position. Close to the wall, f_{dr} always was lower. Not all 18000 samples were uncorrelated, because typically each integral time scale of the turbulence contained 2 to 3 samples, so effectively we have at least 6000 independent samples.

From the obtained velocity data statistical quantities were computed using the following procedure.

First the samples were validated by the BSA's according to the following criterion. As mentioned in Sec. II B, the BSA's compute the frequency of the scattered light by means of a spectral analysis, i.e. the signals's power spectrum is computed. The global maximum in this spectrum corresponds to the dominant frequency, which is the relevant quantity. A LDV sample was accepted only if the global maximum was at least four times as large as the secondary local maximum in the spectrum.

Second, the data were inspected for ''spurious'' data by computing, for each measurement position and velocity component, the mean and the standard deviation of the velocities given by the samples. An individual sample then was disregarded in the further processing if it lay outside the interval (mean ± 10 times the standard deviation). In our case, this resulted in only slight changes in the higher-order statistics near the wall. The number of outliers found per time-series of about 18000 samples was always less than 3, and they occurred only in the time-series measured at positions less than 0.5 mm from the wall. This is a sign of the measurement errors caused by reflections of the laser light by the pipe wall, as discussed at the end of Sec. II A.

Third, the coincidence of the measurements of both components was required. That means that a pair of samples

was validated only if the difference in the arrival times of the two samples (one for the axial and one for the radial direction) was less than a certain coincidence window t_{coinc}. We used for all profile measurements $t_{\text{coinc}}=d/U_b$, where d is the width of the LDV measurement volume in the streamwise direction (i.e., 20 μm), and U_b the bulk velocity in the pipe.

After validation the turbulence statistics were computed according to standard procedures. The mean, root-mean-square, skewness, flatness and Reynolds stress were determined for each radial position r.

All measurements were corrected for the spatial integration of the LDV signals due to the finite size of the measurement volumes following a method proposed by Durst *et al.*[10] (see also den Toonder[9]). Statistical measurement errors were computed following the procedure of Lumley and Panofsky.[11] These errors are depicted at a limited number of radial positions as error bars in the figures presented in Sec. III A. Uncertainties in u_τ are also accounted for in these error bars.

Several checks were performed to verify the accuracy of the profile measurements. Integration of the mean velocity profiles gave a flow rate which corresponded with the measured Q within 0.5%. Also, the relation between u_τ as determined from the pressure difference measurements and the measured flow rate Q always obeyed the Blasius friction law within 0.5%. This is an indication that the flow was indeed fully developed. The latter was also confirmed by comparing the readings of the two pressure transducers, because these indicated a truly linear decrease of the mean pressure as a function of the axial direction.

As we have already indicated at the end of Sec. II A, the computed second and higher-order statistics of the flow at positions extremely close to the wall, i.e. in the region $y^+<5$, suffered from inaccuracies most probably caused by reflections of the laser light. These data were therefore excluded from the final results. Although the mean-velocity profiles showed no direct signs of any accuracy problems in the layer $0<y^+<5$, we nevertheless decided to also exclude these data from the results, for the sake of consistency.

For three Reynolds numbers, spectrum measurements were performed at two radial positions in the pipe. The conditions are listed in Table I. The last column contains the measurement positions in wall units and they roughly correspond to $y^+=12$ and 30.

In the spectrum measurements, the objective was to obtain a data rate f_{dr} as high as possible to be able to determine the power spectrum at high frequencies. Hence, the spectrum measurements were carried out in a way different from the profile measurements. For the former, one needs a full time series to be able to resolve all time-scales, whereas for the latter, one needs uncorrelated data to be able to compute the statistics. In the spectrum measurements the data rate ranged from 1600 Hz for the lowest Reynolds number and close to the wall, to 9000 Hz for the highest Reynolds number and away from the wall. In each measurement, around 196000 samples were gathered for each velocity component. This corresponds to a total measurement time $T=123$ s in the case of $f_{dr}=1600$ Hz, and $T=22$ s for $f_{dr}=9000$ Hz.

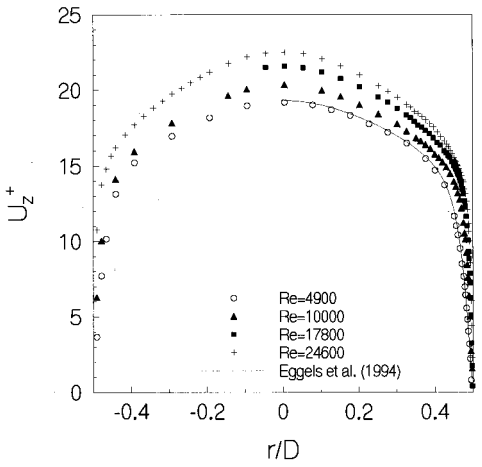

FIG. 4. Mean velocity profiles as measured with LDV for four different Reynolds numbers, compared with the numerical result of Eggels *et al.*[12]

The power spectra were computed from the spectrum measurements as follows. The observed time series, which consisted of approximately 196000 samples distributed in time according to a Poisson random distribution, were re-sampled at equidistant times using linear interpolation between the measured data with the re-sampling frequency equal to the mean data rate of the measurement (f_{dr}). The re-sampled time series then were divided into 186 (± 4) half-overlapping blocks each containing 2048 data points. For each of these blocks, the power spectrum was computed using a FFT and a Bartlett window. The power spectra presented in the following sections were obtained by averaging the spectra of the blocks.

III. RESULTS OF THE LABORATORY EXPERIMENTS

A. Turbulence statistics

We analyse in this section the statistics of the four profile measurements and for the lowest Reynolds number compare them with the results of the direct numerical simulation of Eggels *et al.*[12] Details of the measurement conditions can be found in Table I. The simulation of Eggels *et al.*[12] is a DNS of a pipe flow at Re=5300, which is close to our lowest Reynolds number, Re=4900. The error bars present in the figures for several positions in the pipe were computed according to the method described in Lumley and Panofsky[11] (see also den Toonder[9]).

1. Mean velocity profile

Figure 4 shows the mean velocity profiles, non-dimensionalized with the friction velocity u_τ, along the entire pipe cross section. From the measured profiles that have data points extending from wall to wall (i.e., all profiles except Re=17800), it can be verified that the profiles show the expected symmetric behaviour. The measured data for the lowest Reynolds number show excellent agreement with the DNS profile. In Fig. 5 the same data are plotted in the usual semi-logarithmic manner, using inner scaling. We remind the reader that the friction velocity u_τ was determined from the measured pressure drop, i.e., independently of the velocity profile. The center of the pipe in wall variables is indicated

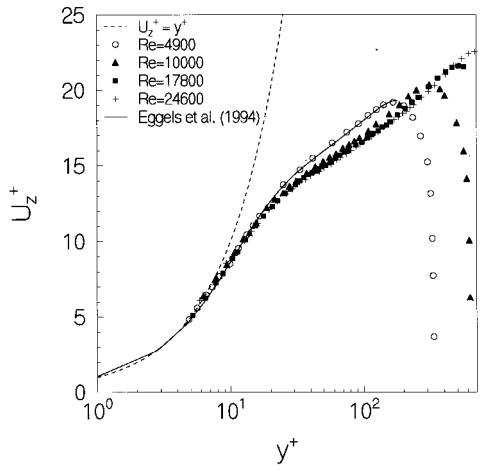

FIG. 5. Measured mean-velocity profile scaled on inner variables. The centre of the pipe is at $y^+ \approx 170$, 315, 520, and 690, respectively, for increasing Re.

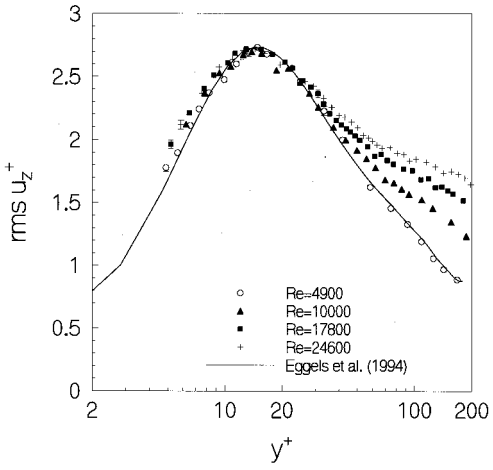

FIG. 7. Measured axial rms profiles scaled on inner variables as a function of Re.

in the caption of the figure. It can be argued, using various arguments, that the mean velocity profile in a turbulent pipe flow at high Reynolds numbers may be described with the following relations (e.g., Tennekes and Lumley[13]):

$$U_z^+ = y^+, \quad \text{if } 0 < y^+ < 5, \tag{3}$$

$$U_z^+ = A \ln y^+ + B, \quad \text{if } y^+ > 30. \tag{4}$$

These equations specify the law of the wall f that has been mentioned in Eq. (1) for various y^+-ranges. The value of the constants A and B still is a matter of dispute, since there is considerable scatter in these values as determined from experiments. For fully developed pipe flow at high Reynolds numbers, the average of all experiments indicate that $A = 2.5$ and $B = 5.0$. However, for low Reynolds numbers the additive constant B takes a value of 5.5, as mentioned in Kim *et al.*[14] Figure 5 shows that all four measured profiles quite nicely tend towards Eq. (3) as the layer $0 < y^+ < 5$ is approached. In the region $y^+ > 30$ our data show a clear Reynolds number dependence that is shown in more detail in Fig. 6. In this figure we have also plotted the logarithmic law given by Eq. (4), with $A = 2.5$ and two different values for the additive constant B, viz. 5.0 and 5.5. At the lowest Reynolds number the data in Fig. 6 confirm the DNS results of Eggels *et al.*[12] For increasing Reynolds numbers, the profile moves in the direction of the line defined by Eq. (4) with $A = 2.5$ and $B = 5.0$, which seems to have been reached for Re=24600. The intermediate profile with Re=10000 corresponds to Eq. (4) with the values recommended by Kim *et al.*[14] for low Reynolds numbers, i.e., $B = 5.5$. The upward deviation of the data from the logarithmic profile at the highest y^+ values in Fig. 6 is due to the fact that here the outer region of the pipe is reached.

2. Rms statistics

The rms values of the axial and the radial velocity fluctuations are depicted in Figs. 7 and 8, respectively.

The axial rms profiles do not show any Reynolds number dependence up to $y^+ \approx 30$, approximately the peak value and the position of the peak are the same for all measurements in support of Mochizuki and Nieuwstadt.[3] Again, the Re=4900 data are in good agreement with the DNS results.

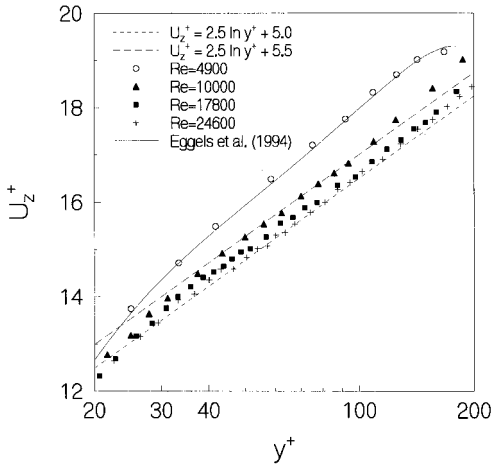

FIG. 6. Detailed view of the logarithmic layer.

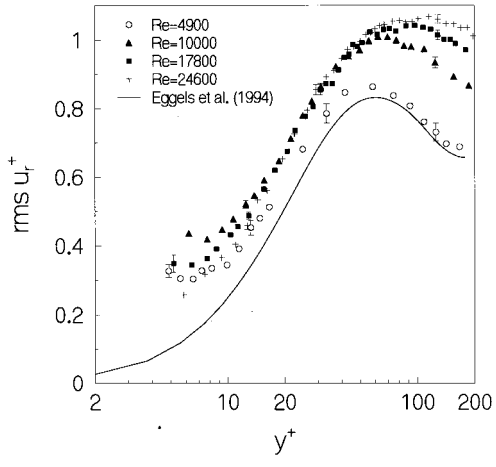

FIG. 8. Measured radial rms profiles scaled on inner variables.

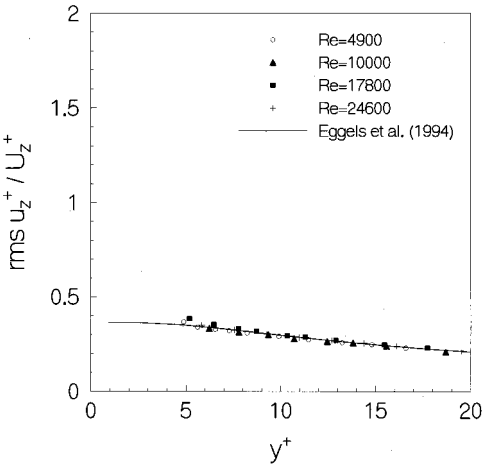

FIG. 9. Measured axial rms profiles, normalized by the local mean velocity.

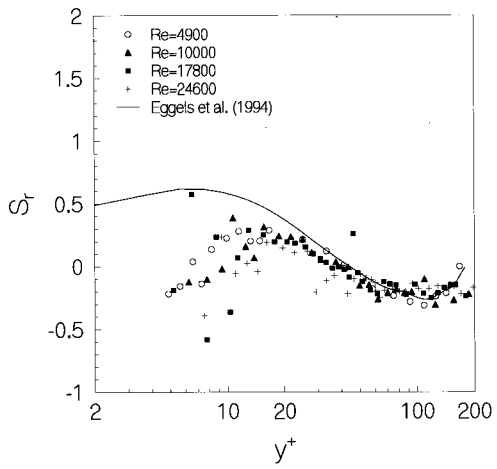

FIG. 11. Measured radial skewness profiles.

For the radial rms profile, a clear Re-dependence can be observed in Fig. 8. With increasing Re, the peak value becomes larger and situated further from the wall. Also, the LDV data differ significantly from the DNS data for the lowest Reynolds number. The upward deviation of the experimental data with respect to the DNS was also found by Westerweel,[15] who used Particle Image Velocimetry to measure turbulent pipe flow, and by Tahitu[16] employing LDV. The difference therefore seems to be a real effect, with the computations underestimating the radial rms velocity. The reason for this underestimation remains unclear. We shall refrain here from speculation on its background. Therefore, this point must be left for further study.

In Fig. 9 the axial rms velocity is normalized by the local mean velocity and plotted only in the near-wall region. This quantity is extremely sensitive to measurement noise. There is excellent agreement between all LDV data and the DNS results of Eggels *et al.*[12] This confirms the good accuracy of the data.

3. Higher-order statistics

We depict the profiles for the skewness in Figs. 10 and 11. The radial skewness close to the wall shows some scatter close to the wall. The cause for this scatter is probably of a statistical nature and we will expand this remark in the next paragraph. In neither of the figures a clear trend with Reynolds number can be observed, except for S_z in the core region of the pipe. S_z has the same general trend as a function of y^+ as the DNS, although the simulations give higher values close to the wall. The trend of S_r for Re=4900, however, is essentially different from the DNS in the near-wall region: the measurements indicate that S_r takes a negative value in the viscous sub-layer, which would be in qualitative agreement with the results of Kim *et al.*[14] for channel flow. But in view of the scatter in the data no definite conclusions can be drawn regarding this matter.

Figures 12 and 13 illustrate the behaviour of the flatness factors. Again, some scatter of the data appears close to the wall, in particular for the radial component. The statistical error, indicated by the error bar, is not able to explain the amount of scatter. However, we note here that our error analysis for the flatness factor is based on the assumption of a Gaussian probability distribution of the data, which clearly is not the case according to the large values of the radial flatness factor close to the wall (that is 3 for a Gaussian

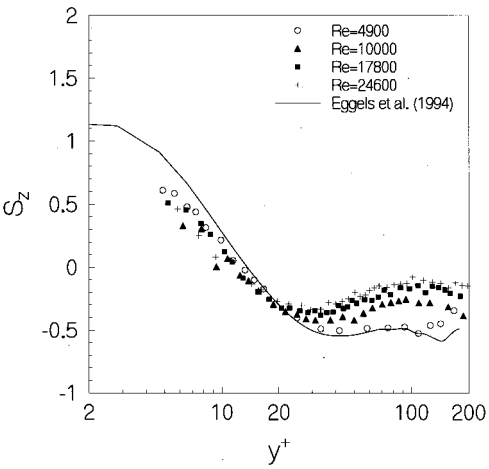

FIG. 10. Measured axial skewness profiles.

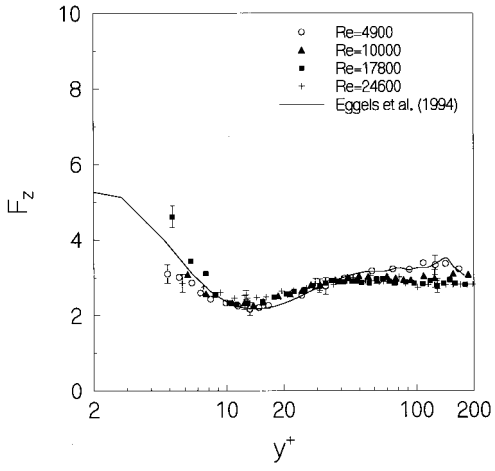

FIG. 12. Measured axial flatness factor.

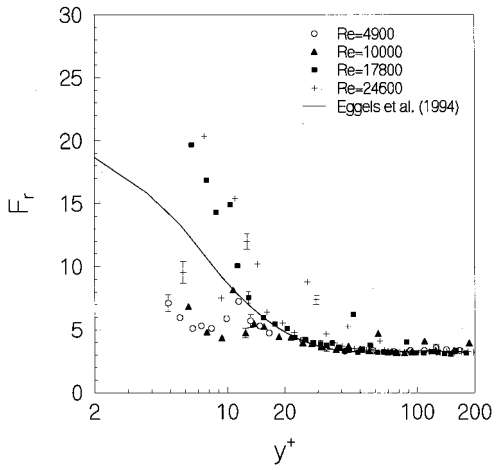

FIG. 13. Measured radial flatness factor.

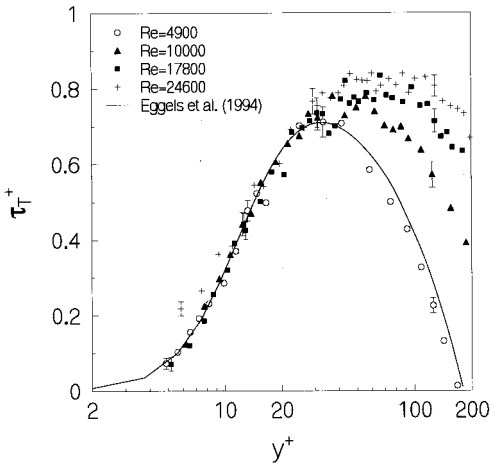

FIG. 14. Measured turbulent shear stress scaled on inner variables.

stochastic process). Hence the statistical error made in approximating the higher-order moments may have been larger. There seems to be no significant Re-dependence for F_z, and the LDV- and the DNS-data are in reasonable agreement. Despite the scatter, the experimental data of Fig. 13 suggest that the radial flatness factor in the near wall region increases as the Reynolds number is increased. The LDV-data for Re=4900 show the same trend as the DNS profile, but the LDV values are smaller. Probably, this is due to the fact that the measurement times and data rates have been too small to be able to capture the very rare events which cause the high flatness factor, as is explained in Xu *et al.*[17] The large radial flatness factor levels near the wall can be explained in terms of the creation of stream-wise vortices as discussed by Xu *et al.*[17] The fact that the flatness factor seems to become larger for increasing Reynolds number may therefore be explained by either an increase in strength of these vorticity structures, or by a more intermittent appearance. The former of these explanations is in accordance with the conclusion of Antonia and Kim,[18] that the strength of the stream-wise vortices in the wall region increases with increasing Re in their simulated low-Reynolds-number channel flow.

4. Shear stresses

The turbulent shear stress τ_T^+ is given in Fig. 14. The influence of the Reynolds number is clear, and the LDV data at the lowest Re are in good agreement with the DNS results. For the shear stresses in a fully developed turbulent pipe flow, the following balance can be derived:

$$2\frac{r}{D}=\tau_T^+ + \tau_V^+, \tag{5}$$

where τ_V^+ is the non-dimensional viscous shear stress, defined as $\tau_V^+ = -dU_z^+/dr^+$. Using the measured mean velocity profile, we computed the viscous shear stress and with this value we obtained the turbulent shear stress according to Eq. (5). The value of the stress thus obtained can be compared to the actually measured value. The result is shown in Fig. 15 for the lowest and the highest Reynolds number, where the dashed lines correspond to the profiles found from the mean velocity gradient and the stress balance. The agreement is quite reasonable, except for a slight under-prediction at the higher Reynolds number. These results confirm our previous statement that the flow can be considered as fully developed.

5. Turbulent energy production

Finally, in Fig. 16 the non-dimensionalized production of turbulent energy is shown, where P_{zz} is defined as

$$P_{zz}=-\tau_T\frac{dU_z}{dr}. \tag{6}$$

This quantity is responsible for the generation of turbulent kinetic energy by extracting energy from the mean flow and transferring this into the axial normal turbulent stress component. Although the scatter is substantial, due to the error in the velocity gradient, Fig. 16 gives no evidence of a Reynolds-number dependence. Furthermore, the agreement with the DNS results at the lowest Reynolds number is good.

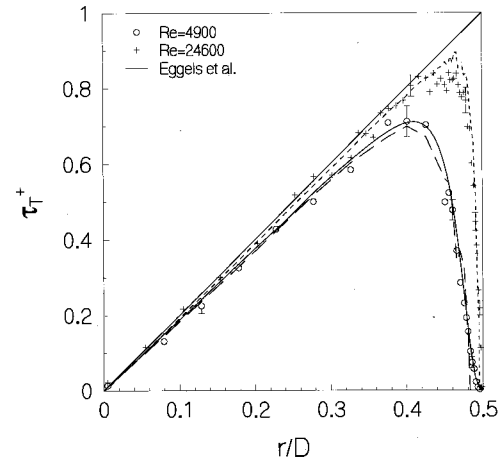

FIG. 15. Measured turbulent shear stress (symbols) and the same quantity as determined from Eq. (5) and the velocity profile (dashed lines).

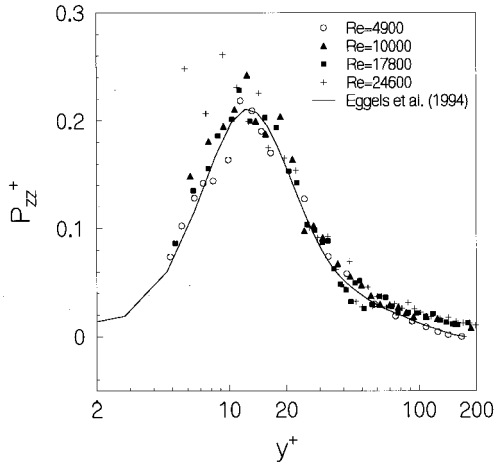

FIG. 16. The dimensionless turbulent energy production scaled on inner variables.

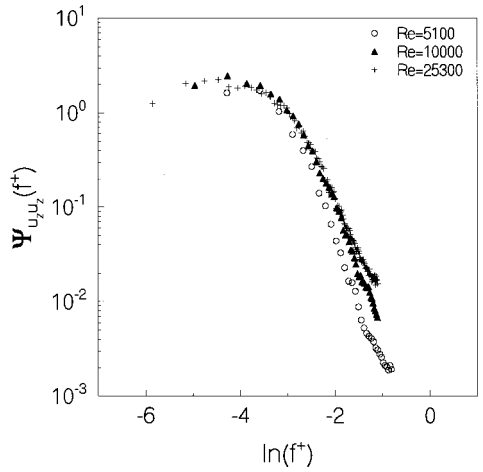

FIG. 18. As the previous figure, with the vertical axis plotted logarithmically.

B. Power spectra

In this section we present the power spectra measured at $y^+ \approx 12$ and 30, for the three Reynolds numbers Re=5100, 10000 and 25300. The results are plotted in the format introduced by Perry and Abell,[5] which was used in the paper of Wei and Willmarth.[4] The abscissa of each plot is the logarithm of the dimensionless frequency, $f^+ = f\nu/u_\tau^2$. The ordinate of each plot is $\Psi_{u_\alpha u_\alpha}(f^+)$, which is defined so that the area beneath a semi-logarithmic plot of $\Psi_{u_\alpha u_\alpha}(f^+)$ is proportional to the mean square of the fluctuating signal, non-dimensionalized on inner variables, i.e.

$$\int \Psi_{u_\alpha u_\alpha}(f^+) d(\ln f^+) = \frac{\overline{u_\alpha u_\alpha}}{u_\tau^2} = \left[\frac{\mathrm{rms}(u_\alpha)}{u_\tau}\right]^2. \tag{7}$$

The relation between $\Psi_{u_\alpha u_\alpha}(f^+)$ and the one-dimensional power spectrum $E_{u_\alpha u_\alpha}(f^+)$ is

$$\Psi_{u_\alpha u_\alpha}(f^+) = \frac{1}{u_\tau^2} f E_{u_\alpha u_\alpha}(f^+). \tag{8}$$

Figures 17–19 show the results for $y^+ \approx 12$. From Fig. 17, it follows that the stream-wise power spectrum at $y^+ \approx 12$ is only slightly influenced by Reynolds number, which is consistent with results of the stream-wise rms shown in Fig. 7. In the energy-containing frequency-range there is considerable scatter but we cannot distinguish a consistent change in the profile with Reynolds number. In the high-frequency range on the other hand, a small but systematic increase of energy as Re increases can be discerned. This effect is more clearly visible in Fig. 18, where this range is emphasized by plotting the vertical axis logarithmically. The increase is so small, however, that it hardly contributes to the total energy.

Figure 19 gives proof of a Reynolds number dependence of the radial power spectrum. The spectrum is enlarged over the entire frequency range as Re increases from 5100 to 10000. The increase of the radial power spectrum as the Reynolds number further increases to 25300 is much less pronounced. These observations are again consistent with the

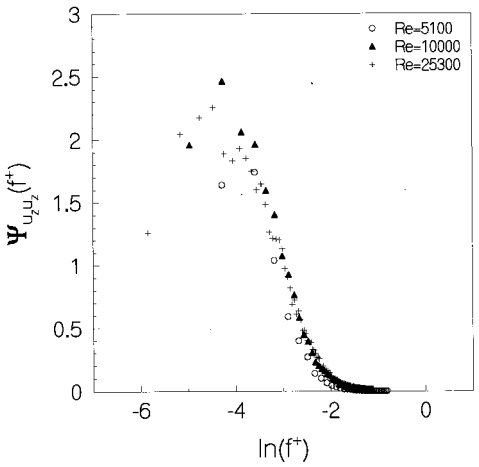

FIG. 17. The power spectrum of the stream-wise velocity fluctuations at $y^+ \approx 12$ for three different Reynolds numbers.

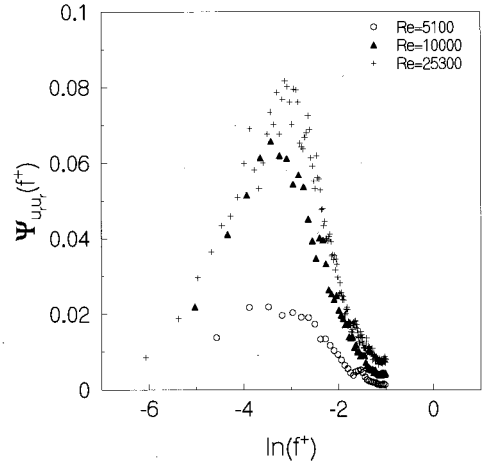

FIG. 19. The power spectrum of the radial velocity fluctuations at $y^+ \approx 12$ for three different Reynolds numbers.

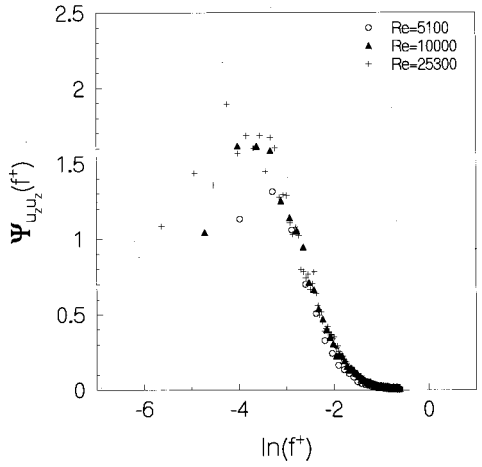

FIG. 20. The power spectrum of the stream-wise velocity fluctuations at $y^+ \approx 30$ for three different Reynolds numbers.

results shown in Fig. 8 for the radial rms of the velocity fluctuations.

It follows from Figs. 20–21 that at $y^+ \approx 30$, the power spectra show about the same behaviour as at $y^+ \approx 12$. The stream-wise power spectrum is only slightly changed at high frequencies. On the other hand, the radial power spectrum shows a strong Reynolds number dependence, that is even more clear than at $y^+ \approx 12$. Especially the difference between the two highest Reynolds numbers is more pronounced than at $y^+ \approx 12$. Again, with an increase of Re, the radial energy is increased over the entire frequency range.

IV. CONCLUSIONS AND DISCUSSION

We have performed LDV profile measurements of a turbulent pipe flow of water at Re=4900, 10000, 17800 and 24600, corresponding to Re_τ=338, 629, 1040 and 1380, respectively. The results have been compared, using inner scaling. The conclusions from these measurements can be summarized as follows.

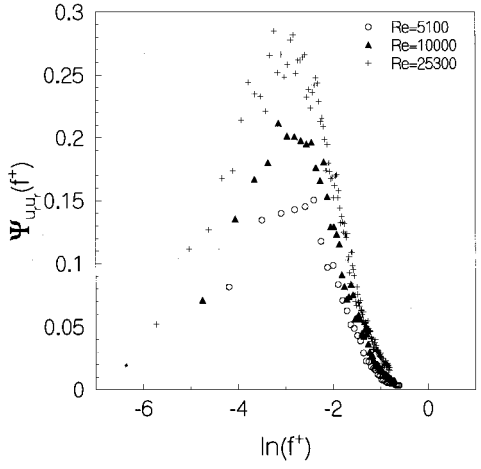

FIG. 21. The same as the previous figure, for the radial fluctuations.

There is a clear Reynolds-number dependence for the mean velocity profile non-dimensionalized with wall variables in the logarithmic region for Re<25000. The ''universal'' logarithmic law with slope 2.5 and additive constant 5.0, seems to be valid only for Re>25000, approximately. For Reynolds number smaller than 25000, the additive constant increases with decreasing Re, and for the lowest Reynolds numbers also the slope becomes larger, in agreement with the DNS results of Eggels *et al.*[12]

The rms of the axial or stream-wise velocity fluctuations has no significant Re-dependence in the near-wall region when inner scaling is used, i.e. its value and peak position are not influenced by the Reynolds number. The radial turbulence intensity, however, increases with increasing Re, and its peak position shifts away from the wall.

The higher-order turbulence statistics show no clear dependence on the Reynolds number, although the radial flatness factor seems to be enlarged in the region close to the wall as Re is increased. This may have some consequences for the near-wall coherent structures.

The Reynolds stress scales on inner variables up to $y^+ \approx 30$. Further away from the wall, the results for the different Reynolds numbers diverge, causing the peak of the Reynolds stress profile to increase and its position to shift towards larger y^+.

We also performed spectrum measurements at $y^+ \approx 12$ and $y^+ \approx 30$ for the Reynolds numbers 5100, 10000 and 25300. The results can be summarized as follows.
At both positions, the stream-wise power spectrum, non-dimensionalized with inner variables, does not show a substantial Reynolds number dependence. Only at the highest frequencies a slight but a consistent increase of energy with increasing Re may be discerned.

The radial power spectrum exhibits a clear increase of energy over the entire frequency domain if the Reynolds number is enlarged. This effect is particularly noticeable at $y^+ \approx 30$.

The fact that we find a clear Reynolds number dependence for the mean-velocity profile scaled on inner variables is in contradiction with the channel flow results of Wei and Willmarth,[4] and with the conclusions of the channel flow and boundary layer review by Gad-el-Hak and Bandyopadhyay.[1] These authors argue for a Reynolds-number independent logarithmic profile with the constants $A=2.44$ and $B=5.5$. On the other hand, these references claim that the stream-wise turbulence intensity scales on inner variables only up to $y^+ \approx 12$, whereas we find a larger region of similarity, viz. up to $y^+ \approx 30$. Our results agree with the cited papers with respect to the Re-dependence of the Reynolds stress and the normal velocity fluctuations. The dependence of the Reynolds stress we find is not surprising, since, if we assume that its maximum is in the logarithmic region, it can be easily shown from Eqs. (4) and (5) that the peak of τ_T^+ should increase and shift away from the wall with increasing Re_τ. Our measured power spectra show the same tendencies as those presented in Wei and Willmarth.[4] The differences between our pipe flow results and the channel and boundary layer data reported in the literature may well be explained by

the differences in geometry which at low Reynolds numbers, where turbulent flow structures are still relatively large, may influence statistics. This explanation implies also, that the notion of an inner layer in which the flow geometry is not important may be too simple especially at low Reynolds numbers.

In conclusion, we can say that our data give proof of a clear Reynolds number dependence of turbulence statistics scaled on inner variables in turbulent pipe flow for low to moderate Reynolds numbers. As the Reynolds number increases, the scaled quantities seem to approach an asymptotic value. Whether this effect indeed appears, and inner scaling hence might be valid for higher Reynolds numbers, should be investigated in the future by performing measurements at larger Reynolds numbers. In fact, a range of higher Reynolds numbers that links up with the range presented in the present paper is currently subject of study in the so-called ''superpipe'' facility at Princeton University.[19]

ACKNOWLEDGMENTS

We acknowledge the support of the Foundation for Fundamental Research on Matter (FOM). We thank Dr. Aswin A. Draad for his invaluable advice and support during the experiments. Also, Gabriël Tahitu and Edo Koevoet are thanked for their help in performing the measurements. Finally, we would like to thank the reviewers for their valuable suggestions that have lead to a significant improvement of the paper.

APPENDIX: BARENBLATT'S SCALING LAW AT LOW Re

Barenblatt[20] develops a view on flow similarity in turbulent shear flow that is different from the inner scaling approach mentioned in the present paper. Barenblatt proposes an alternative scaling law for the logarithmic law, Eq. (4). His scaling law is non-universal in that it depends on the Reynolds number. It reads as

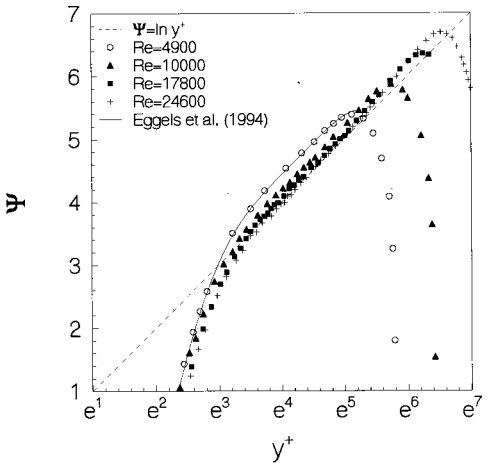

FIG. 22. Measured mean velocity data scaled following the law of Barenblatt.

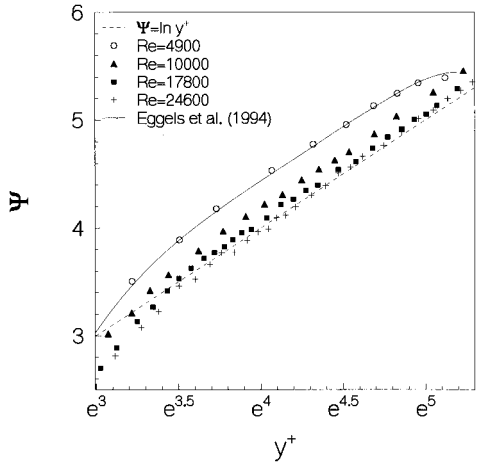

FIG. 23. Detailed view of the previous figure.

$$U_z^+ = \left(\frac{1}{\sqrt{3}} \ln \mathrm{Re} + \frac{5}{2} \right) (y^+)^{3/(2 \ln \mathrm{Re})}. \tag{A1}$$

Simple transformations reduce Eq. (A1) to a quasi-universal form involving a new function $\Psi(U_z^+)$, viz.

$$\Psi = \frac{1}{\alpha} \ln \frac{2\alpha U_z^+}{\sqrt{3} + 5\alpha} = \ln y^+, \quad \alpha = \frac{3}{2 \ln \mathrm{Re}}. \tag{A2}$$

This means that if Eqs. (A1) and (A2) are true, then all experimental points should settle down on one single straight line in the $(\Psi, \ln y^+)$-plane, viz. on the bisectrix of the first quadrant.

In Barenblatt and Prostokishin,[21] the above scaling law is tested with experimental data from Nikuradze.[22] The overwhelming majority of these experimental points confirm the validity of Eq. (A2).

Our LDV data obtained in the turbulent pipe flow at low to moderate Reynolds numbers are plotted in the $(\Psi, \ln y^+)$-plane in Figs. 22 and 23. It is clear that the data at the lowest Reynolds numbers deviate significantly from the law, Eq. (A2). Figure 23 shows that the correspondence improves with increasing Reynolds number. For Re≈25000, there is good agreement between the measured data and the scaling law over a considerable y^+-range. It should be noted that Figs. 22 and 23 are remarkably similar to Figs. 5 and 6, which show the classical inner scaling of the mean velocity data.

From this analysis, we must conclude that Barenblatt's scaling law is not confirmed for low Reynolds numbers by our experiments. Only when Re≈25000 is reached, the experimental data coincide well with the scaling law. This conclusion is essentially the same as that for the universal logarithmic scaling law.

[1] M. Gad-el Hak and P. R. Bandyopadhyay, ''Reynolds number effects in wall-bounded turbulent flows,'' Appl. Mech. Rev. **47**, 307 (1994).

[2] P. Bradshaw and G. P. Huang, ''The law of the wall in turbulent flows,'' Proc. R. Soc. London Ser. A **451**, 165 (1995).

[3] S. Mochizuki and F. T. M. Nieuwstadt, ''Reynolds-number-dependence of the maximum in the streamwise velocity fluctuations in wall turbulence,'' Exp. Fluids **21**, 218 (1996).

[4] T. Wei and W. W. Willmarth, ''Reynolds-number effects on the structure

of a turbulent channel flow,'' J. Fluid Mech. **204**, 57 (1989).
[5]A. E. Perry and C. J. Abell, ''Scaling laws for pipe flow turbulence,'' J. Fluid Mech. **67**, 257 (1975).
[6]A. A. Draad, ''Laminar–turbulent transition in pipe flow for Newtonian and non-Newtonian fluids,'' Ph.D. thesis, Delft University of Technology, 1996.
[7]F. Durst, A. Melling, and J. H. Whitelaw, Principles and Practice of Laser–Doppler Anemometry (Academic Press, New York, 1976).
[8]B. Ruck, Laser-Doppler-Anemometry AT-Fachverlag GmbH, Stuttgart, 1987.
[9]J. M. J. den Toonder, ''Drag reduction by polymer additives in a turbulent Pipe flow: Laboratory and numerical experiments,'' Ph.D. thesis, Delft University of Technology, 1995.
[10]F. Durst, J. Jovanovic, and J. Sender, ''Detailed measurements of the near wall region of turbulent pipe flow,'' in D. Goldstein, D. Hughes, R. Johnson, and D. Lankford, editors, Data for Validation of CFD Codes (ASME, New York, 1993).
[11]J. L. Lumley and H. A. Panofsky. The Structure of Atmospheric Turbulence (Interscience, New York, 1964).
[12]J. G. M. Eggels, F. Unger, M. H. Weiss, J. Westerweel, R. J. Adrian, R. Friedrich, and F. T. M. Nieuwstadt, ''Fully developed turbulent pipe flow: A comparison between direct numerical simulation and experiment,'' J. Fluid Mech. **268**, 175 (1994).
[13]H. Tennekes and J. L. Lumley, A First Course in Turbulence (MIT Press, Cambridge, 1972).
[14]J. Kim, P. Moin, and R. Moser, ''Turbulence statistics in fully developed channel flow at low Reynolds number,'' J. Fluid Mech. **177**, 133 (1987).
[15]J. Westerweel, ''Digital Particle Image Velocimetry—Theory and application,'' Ph.D. thesis, Delft University of Technology, 1993.
[16]G. J. R. Tahitu, ''The possibilities of LDA measurements in a turbulent pipe flow,'' Master's thesis, Delft University of Technology, 1994, Report MEAH-117 (in Dutch).
[17]C. Xu, J. M. J. den Toonder, F. T. M. Nieuwstadt, and Z. Zhang, ''Origin of high kurtosis levels in the viscous sublayer. Direct numerical simulation and experiment,'' Phys. Fluids **8**, 1938 (1996).
[18]R. A. Antonia and J. Kim, ''Low-Reynolds-number effects on near-wall turbulence,'' J. Fluid Mech. **276**, 61 (1994).
[19]M. V. Zagarola, ''Mean-flow scaling of turbulent pipe flow,'' Ph.D thesis, Princeton University, 1996.
[20]G. I. Barenblatt, ''Scaling laws for fully developed turbulent shear flows. Part 1. Basic hypotheses and analysis,'' J. Fluid Mech. **248**, 513 (1993).
[21]G. I. Barenblatt and V. M. Prostokishin, ''Scaling laws for fully developed turbulent shear flows. Part 1. Processing of experimental data,'' J. Fluid Mech. **248**, 521 (1993).
[22]J. Nikuradze, ''Gesetzmässigkeiten der turbulenten Strömung in glatten Röhren,'' VDI Forschungsheft, 1932, No. 356.